AEROSPACE REPORT NO.
TR-2007(8555)-3

# X-Ray Dose in Microfocus Radiographic Inspections

15 March 2007

Prepared by

G. W. STUPIAN
Electronics and Photonics Laboratory
Laboratory Operations

Prepared for

SPACE AND MISSILE SYSTEMS CENTER
AIR FORCE SPACE COMMAND
483 N. Aviation Blvd.
El Segundo, CA 90245-2808

Engineering and Technology Group

THE AEROSPACE CORPORATION
El Segundo, California

This report was submitted by The Aerospace Corporation, El Segundo, CA 90245-4691, under Contract No. FA8802-04-C-0001 with the Space and Missile Systems Center, 483 N. Aviation Blvd., El Segundo, CA 90245. It was reviewed and approved for The Aerospace Corporation by B. Jaduszliwer, Principal Director, Electronics and Photonics Laboratory; and D. C. Marvin, Principal Director, Office of Research & Technology Applications. Michael Zambrana was the project officer for the Mission-Oriented Investigation and Experimentation (MOIE) program.

This report has been reviewed by the Public Affairs Office (PAS) and is releasable to the National Technical Information Service (NTIS). At NTIS, it will be available to the general public, including foreign nationals.

This technical report has been reviewed and is approved for publication. Publication of this report does not constitute Air Force approval of the report's findings or conclusions. It is published only for the exchange and stimulation of ideas.

Michael Zambrana
SMC/EA

# REPORT DOCUMENTATION PAGE

*Form Approved*
*OMB No. 0704-0188*



| 1. REPORT DATE (*DD-MM-YYYY*) | 2. REPORT TYPE | 3. DATES COVERED *(From - To)* |
|---|---|---|
| 15-03-2006 | | |

**4. TITLE AND SUBTITLE**

X-Ray Dose in Microfocus Radiographic Inspections

**5a. CONTRACT NUMBER**
FA8802-04-C-0001

**5b. GRANT NUMBER**

**5c. PROGRAM ELEMENT NUMBER**

**6. AUTHOR(S)**

G. W. Stupian

**5d. PROJECT NUMBER**

**5e. TASK NUMBER**

**5f. WORK UNIT NUMBER**

**7. PERFORMING ORGANIZATION NAME(S) AND ADDRESS(ES)**

The Aerospace Corporation
Laboratory Operations
El Segundo, CA 90245-4691

**8. PERFORMING ORGANIZATION REPORT NUMBER**

TR-2007(8555)-3

**9. SPONSORING / MONITORING AGENCY NAME(S) AND ADDRESS(ES)**

Space and Missile Systems Center
Air Force Space Command
483 N. Aviation Blvd.
El Segundo, CA 90245

**10. SPONSOR/MONITOR'S ACRONYM(S)**
SMC

**11. SPONSOR/MONITOR'S REPORT NUMBER(S)**

**12. DISTRIBUTION/AVAILABILITY STATEMENT**

Approved for public release; distribution unlimited.

**13. SUPPLEMENTARY NOTES**

**14. ABSTRACT**

The radiation dose accumulated by specimens during real-time microfocus radiographic examination is of interest to program office customers and their contractors because of possible damage to certain sensitive types of electronic components. The real-time X-ray facility in The Aerospace Corporation's Laboratory Operations has two microfocus radiography systems. This report characterizes the radiation levels in both our Feinfocus model 160.52 system and our Phoenix X-ray "PCBAlAnalyzer." These instruments are representative of the state-of-the-art in X-ray inspection.

The variables involved in the determination of total dose include the voltage and current of the X-ray tube; the amount and type of shielding material (incidental and deliberate) between the sample and the X-ray source; the distance from the source to the sample; and the time spent looking at the sample. Some general principles of X-ray dosimetry are discussed along with strategies for dose minimization when required.

Most of the considerable body of published work on the characterization of kilovolt X-ray sources has been done by the medical physics community. This report aims at ensuring that similar information is brought to the attention of people in the aerospace industry.

**15. SUBJECT TERMS**

Microfocus radiography, Real-time X-ray, X-ray dose

| 16. SECURITY CLASSIFICATION OF: | | | 17. LIMITATION OF ABSTRACT | 18. NUMBER OF PAGES | 19a. NAME OF RESPONSIBLE PERSON |
|---|---|---|---|---|---|
| a. REPORT | b. ABSTRACT | c. THIS PAGE | | | Gary Stupian |
| UNCLASSIFIED | UNCLASSIFIED | UNCLASSIFIED | | 27 | 19b. TELEPHONE NUMBER *(include area code)* (310)336-6466 |

## Acknowledgements

The support of colleagues in the Electronic Materials and Devices section, Microelectronics Technology Department, of the Electronics and Photonics Laboratory, particularly Mr. Neil A. Ives and Dr. Martin S. Leung, is gratefully acknowledged.

## Contents

## Figures

## Tables

# 1. Introduction

The microfocus radiography systems in the Electronics and Photonics Laboratory (EPL) in Laboratory Operations have proven to be extremely valuable tools for the investigation of a wide range of problems for program office and commercial customers. Samples of many different types, including both electronic and mechanical components, are routinely investigated. X-ray radiation has no noticeable effect on many of the components that we examine. Some electronic components are, however, sensitive to ionizing radiation, and customers frequently inquire about the radiation dose to which a sample will be subjected during an X-ray inspection. This report summarizes dose rate measurements made in our laboratory on our two X-ray systems. One of our systems uses a directional-type X-ray tube while the other uses a transmission-type tube (these terms will be explained shortly). These two X-ray systems are representative of most of the instruments currently in general use for microfocus radiography.

X-ray dose rates are readily measured with suitable instruments. The first question one might ask is whether the measured numbers are "reasonable" for a particular X-ray system. A second issue is more subtle. People typically inquire about the total dose that will be accumulated by their silicon (or other semiconductor) microelectronic devices. The quantitative determination of doses to components, especially within packages, is a complicated issue. The energy spectrum of the X-ray radiation must be taken into account. Any intervening material, such as lids on semiconductor packages, can reduce the dose. In certain situations, e.g., for gold metallization on a semiconductor substrate, the dose in the semiconductor can actually be enhanced over the value that would be found for absorption of radiation by silicon alone.

Fortunately, several methods for calculating the intensity and the spectral distribution of the radiation produced by X-ray sources are available. The corresponding computer codes can be used both to provide a "sanity check" on the dose measurements and to provide a connection between X-ray doses measured with, e.g., an ionization chamber meter and the corresponding doses in silicon or other materials of interest. One can, in principle, measure dose rates in a package directly if a small sensor such as a thermoluminescent dosimeter (TLD) can be inserted in the device being examined or in a representative test device. In practice, this method presents certain difficulties. We believe that measurements of the dose in air delivered by an X-ray machine, combined with calculations of the dose absorbed by specific components made of other materials, can provide accurate answers to total dose questions.

The terms "X-ray dose" and "dose rate" have both been used in this introduction. "Dose" is the dose rate multiplied by the exposure time. This report is concerned with the total dose during the time (typically minutes to at most a few hours) that is required for a radiographic examination. It is often easier to talk about a normalized quantity, i.e., the dose rate. Most numbers cited in this report will be stated as dose rates. Note that there are actual "dose rate" effects. The response of a component may depend on whether the total dose is delivered quickly or slowly. Such dose rate effects are beyond the scope of this report.

We first discuss the design of our microfocus X-ray tubes. While not strictly necessary to our primary goal of quantifying X-ray dose, some knowledge of tube construction will aid in understanding of the data to be presented.

# 2. Background

## 2.1 Our X-Ray Systems

Our first microfocus X-ray system, a model FXS 160.52 manufactured by Feinfocus Roentgen-Systeme GMBH, Garbsen, Germany (now a subsidiary of Comet AG, Flamatt, Switzerland), has been in operation since late 1994. Figure 1 shows the system in our laboratory. Our newer system, a "PCBA|Analyzer" manufactured by Phoenix X-ray Systems + Services GMBH, Wunstorf, Germany (Figure 2), is on the other side of the room.

The two instruments share some features common to all real-time X-ray systems but also have different and complementary characteristics. The Feinfocus instrument is physically larger. The X-ray cabinet with its 70 cm x 60 cm access door is seen at the left in Figure 1. Specimens weighing up to 30 kg (66 lb) can be accommodated. We have successfully examined objects weighing over 30 kg although the physical limitations of the manipulator stage and cabinet may require specimen repositioning during the analysis to increase the total volume that can be brought into the field of view. The Phoenix system is physically smaller and more limited in sample size, but has higher ultimate spatial resolution.

The maximum beam accelerating potential in the Feinfocus system is 200 kV and is adjustable in 1-kV increments. The current in the beam is adjustable in 1 μA steps. The current and voltage are chosen for best results and are often altered to highlight different features during a single investigation. The power in the electron beam is, of course, the accelerating voltage times the electron beam current. The Feinfocus tube is rated at 320 W and is water cooled, although we seldom run above 40 W. The Phoenix system has a maximum accelerating potential of 160 kV. Tube current and voltage are again adjustable.

Figure 1. Feinfocus model 160.52 X-ray system.

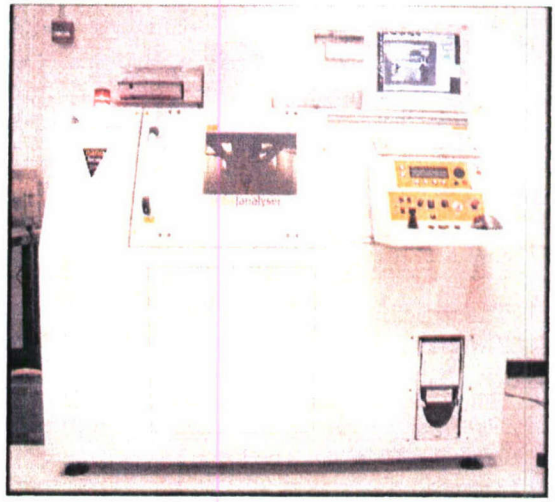

Figure 2. Phoenix X-ray Systems PCBA|Analyzer X-ray system.

The Feinfocus system employs a directional X-ray tube, while the Phoenix system is based on a transmission tube.

## 2.2 Principles of Microfocus Radiography

A schematic diagram of the Feinfocus system is shown in Figure 3. Electrons emitted by a heated tungsten filament are accelerated by an applied voltage. The electron beam is focused and impinges on a tungsten anode in a small spot. A fraction of the energy of the incident electrons (about 0.5% for 100 kV electrons on a tungsten target) is converted into X-radiation by the Bremsstrahlung process and by fluorescent emission. The X-rays diverge from the nearly point source, and an X-ray "shadow" of the sample is cast on a detector, an image intensifier in the Feinfocus instrument. The image intensifier converts the X-ray shadow image into a visible light image on a phosphor screen. A TV camera makes the image on the phosphor available for viewing at video frame rates or for recording. Still images can be captured and saved by computer at the full resolution of the camera. In its present configuration, the Feinfocus system has two switch-selectable cameras. One camera has a 1008 x 1008 pixel 10-bit grayscale output with a video frame rate of 30 frames/s. Some additional magnification is provided by a remotely adjustable optical lens between the phosphor screen and the video camera at the back of the image intensifier. This lens also has a remotely adjustable iris that is very convenient for setting the brightness of the video image. The other camera provides 1024 x 1024 pixel 12-bit grayscale images at 15 frames /s. It is used for computed tomography. An upgrade to a 14-bit solid-state detector array is planned. Microfocus systems are commonly referred to as "real-time" X-ray systems since their X-ray image output can be viewed as the data are acquired. Real-time imaging is often the key to a successful X-ray analysis. The ability to make precise adjustments to the position of the sample can reveal features, such as cracks, that might well be missed in a film-based X-ray system in which only a few images at a small number of viewing angles might be obtained.

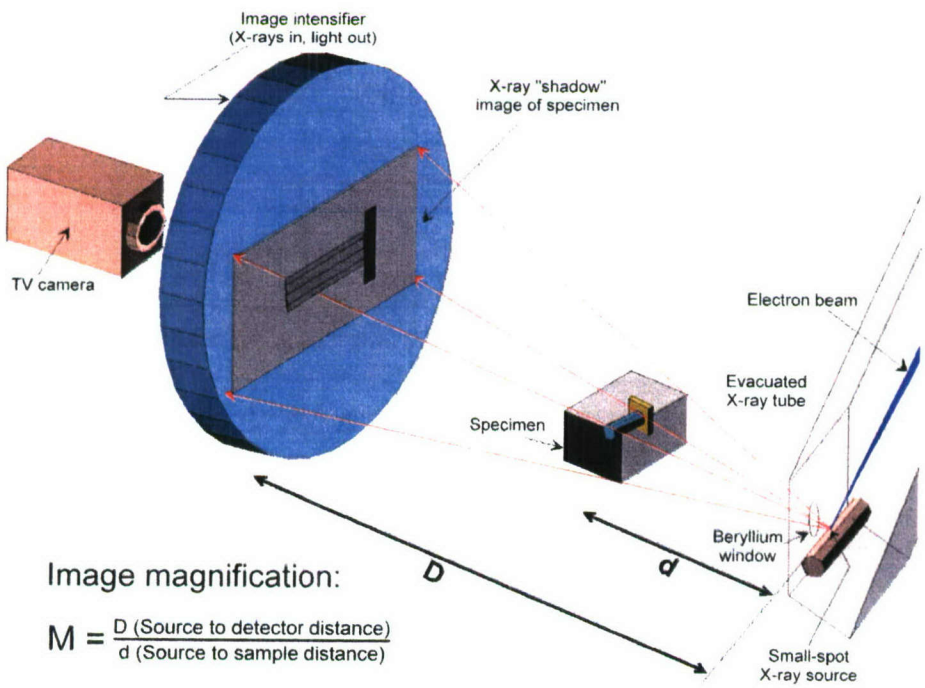


Figure 3. Schematic drawing of the Feinfocus X-ray system.

In general, the higher the beam voltage, the greater the penetrating power of the X-rays; i.e., images can be obtained through greater thicknesses of material. The higher the current, the better the signal-to-noise ratio of the image; i.e., the picture is less "grainy." As is so often the case, there are trade-offs in the selection of these parameters.

A film-based X-ray machine typically has an X-ray source with an area relatively large compared to the size of details to be resolved within the sample. The specimen must therefore be placed against the film to achieve sharp feature definition given the finite size of the source. If image magnification is desired, the developed negative is viewed through a magnifying lens. A microfocus X-ray system provides "geometric" magnification, which is just the ratio of the distance from the focal spot to the image intensifier to the distance between the focal spot and the sample (Figure 3). The magnification will ultimately be limited by the finite size of the X-ray source, as illustrated in Figure 4. In our Feinfocus system, the source spot, the electron beam's footprint on the cylindrical anode, is an ellipse with major and minor axes roughly 7 μm x 4 μm long, respectively, in the microfocus mode when the power in the beam is 8 W or less. The anode is positioned about 6 mm behind a beryllium exit window. The best spatial resolution is obtained with the smallest focal spot (the microfocus mode). If the beam power is increased, the system's control electronics automatically defocus the beam to preclude melting of the tungsten anode. A larger beam spot means that the spatial resolution is in principle decreased although finite spot size is a limitation only at high geometric magnification. The anode in a directional tube can be water cooled, which allows the tube to be run at higher power.

The Phoenix system and the Feinfocus system are very similar conceptually, although there are differences in implementation. The Phoenix system is built around a transmission-type tube. The electron beam is incident perpendicular to the surface of a thin anode consisting of 6 μm of tungsten supported on a 400 μm beryllium exit window. There are reasons for the choice of 6 μm as the anode

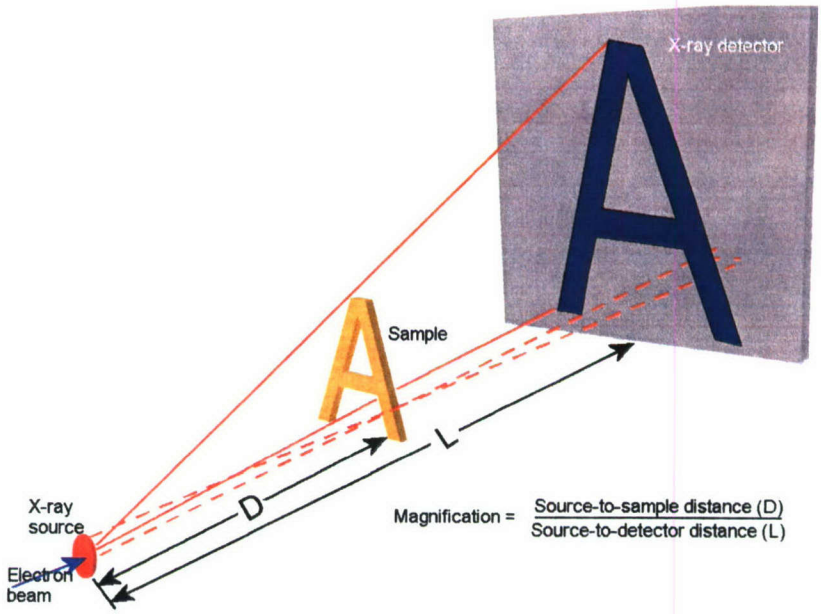


Figure 4 The finite size of the electron beam's focal spot leads to "geometric unsharpness" in the image at high magnifications.

thickness, as we shall see. Very high geometric magnification can be achieved with the Phoenix system for samples small enough to be brought up very close to the target since the minimum source-to-object distance is only about 0.4 mm compared to the minimum 5 mm distance achievable with our Feinfocus directional tube. The Phoenix system also has a smaller focal spot than does the Feinfocus system. In its "microfocus" mode, the Phoenix system's focal spot is about 2 μm in diameter. Note also that the focal spot is circular rather than elliptical since the electron beam is normally incident on the anode. The circular focal spot also contributes to better spatial resolution. The structure of the anode precludes water cooling.

As mentioned, a successful real-time X-ray examination almost always requires viewing a specimen from several different perspectives, and a high-quality sample manipulation system is a critical system requirement. Both the sample and the detector in the Feinfocus instrument are movable using motor controls at the operator's console, although the source is fixed. The sample is mounted on a 5-axis (x, y, z, rotate, and tilt) manipulator. The detector can be moved toward and away from the source. Magnification increases linearly as the source-to-detector distance increases, while the detected signal decreases as $1/(\text{source-detector distance})^2$.

The tube is mounted vertically in our Phoenix system, and X-ray radiation is directed downward, toward the bottom of the cabinet. As in the Feinfocus system, the tube is fixed in position. The sample stage moves laterally (in the x- and y-directions) and vertically (z-axis, toward and away from the tube). The z-axis motion is used to control the magnification. The system is well suited for the examination of reasonably flat objects, such as circuit boards. A solar panel measuring 102 cm x 76 cm (40 x 30 in.) was once inspected, albeit with some difficulty. A rotating chuck can be quickly mounted on the sample manipulator stage to provide 360° rotated views of smaller samples. The Phoenix system also allows the viewing angle to be changed by moving the detector through a 46° arc at a constant source-detector distance. A sample must be close to the X-ray source to obtain high geometric magnification. If the sample is rotated at the highest magnification, it might strike the face of the tube. If the sample is moved away to avoid hitting the face of the tube, the geometric magnification will decrease. The moveable detector overcomes this problem in part. Although some lateral motion of the sample is required to keep the same features in the field of view, the source-sample distance can still be kept relatively short, and thus the image magnification is maintained (Figure 5).

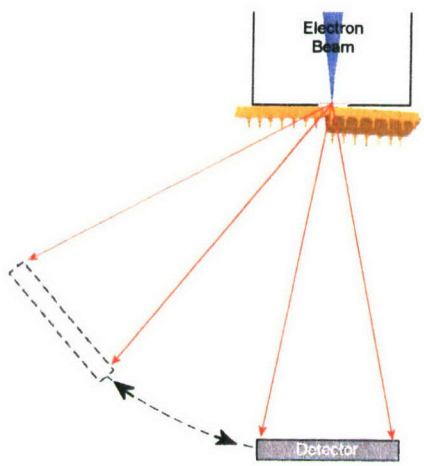


Figure 5. The transmission tube. By tilting the detector, an angled view of the specimen is obtained.

The Phoenix system is equipped with both an image intensifier combined with an 8-bit video camera, and a 16-bit, 512 x 512 pixel solid-state X-ray detector. The increase in dynamic contrast range provided by the solid-state detector is often as important as the increased spatial resolution that results from a smaller focal spot size.

In the microfocus mode, the Phoenix X-ray spot is automatically defocused when anode power exceeds 4 W. The Phoenix system also boasts a "nanofocus" operating mode in which the focal spot can be as small as 0.6 μm. The nanofocus spot is achieved, in part, through collimation with, of course, a corresponding loss of beam intensity. The microfocus and nanofocus anodes and collimating structures are constructed as interchangeable tube heads. Venting the tube to air and switching the heads is a routine procedure that takes 20 to 30 min. It should be pointed out that both our Feinfocus and Phoenix systems use "open" X-ray tube designs. Turbomolecular pumps maintain the internal vacuum necessary for operation. Open-tube systems, although more expensive than closed (sealed) X-ray tubes, have the advantage that filaments and other components can be replaced in the field. The dual-head architecture of the Phoenix nanofocus/microfocus system requires an open-tube design. We should perhaps explicitly state that the X-ray cabinet interiors are at atmospheric pressure in both systems!

## 2.3 Dosimetry

The essential information required for the characterization of an X-ray system is the X-ray dose rate as a function of tube current, tube voltage, and distance from the source. For a microfocus X-ray system, the dose rate must decrease as $1/r^2$, where r is the source-to-object distance. The effects of various source filters on dose are also of interest as we shall see.

### 2.3.1 Units

The Roentgen is a unit still commonly encountered as a measure of radiation. A Roentgen (R) is defined as the quantity of X- or gamma radiation that produces a charge of $2.58 \times 10^{-4}$ coulombs in one kilogram of dry air at 0°C. Although the definition as stated in SI units may seem a bit arbitrary, it is equal to 1 esu/cm$^3$ in the older cgs units. The Roentgen is defined only for ionization produced by photons in air. In most applications, radiation effects in other materials (e.g., silicon, human tissue, etc) are of primary interest, and the energy deposited per unit mass is a more meaningful measure of dose. A dose of 1 rad is defined as an energy deposition of 100 erg/g of material. The official SI dose unit is the Gray, but the rad is still widely employed (1 Gy = 1 joule/kg = 100 Rad). The average energy to create an ion pair in air is 33.97 electron volts (1 eV = $1.602 \times 10^{-19}$ joules), and therefore 1 Roentgen (R) = 0.876 Rad (air). The energy deposited in a sample by X-rays (or other sources of radiation) is dependent on the sample as well as on the spectral distribution of the radiation. Our interest in this report is primarily in silicon and other semiconducting materials, and the intent is ultimately to relate X-ray doses in Roentgens or rad (air) measured in the chamber to rad (Si) absorbed by the sample.

### 2.3.2 Test Instrumentation

This study made use primarily of a Radcal model 2026C ionization chamber meter.[1] This instrument has a small polyethylene air chamber with a volume of 0.18 $cm^3$ on the end of a 3-m cable. The cable plugs into a preamplifier, which, in turn, is connected to a readout unit. The dose rate is read from a digital display. The meter can indicate either dose rate or the total dose received. The units are jumper selectable as either R or Gy(air). The Radcal meter had been serviced and was in calibration at the time of the measurements of the X-ray systems.

# 3. System Characterization – Experimental Results

## 3.1 Feinfocus

### 3.1.1 Dose vs. Distance

A typical dose rate vs distance measurement, taken with the ionization chamber meter, is shown in Figure 6 for a beam energy of 100 kV and a beam current of 80 μA. The Feinfocus tube is, for practical purposes, a point X-ray source For a point source, the flux must fall off as $1/r^2$, at least in the absence of any energy-dependent absorption of X-radiation by air. The measured dose rate was fit to a power law expression:

$$\text{dose rate}(R/\text{min}) = \frac{A}{r^n}, \tag{1}$$

where r is the distance in cm from the X-ray source. Data obtained at various energies at constant power (voltage x current = 8 W) are summarized in Table 1. The power-law fit was calculated using an Excel spreadsheet. The measured dose indeed falls off as $1/r^2$ within experimental error. The $1/r^2$ dependence is more obvious when the dose rate is plotted vs. $1/r^2$, as in Figure 7. We customarily operate the Feinfocus tube at 8 W. At higher power levels, the X-ray system's control electronics broadens the focal spot to guard against local melting of the anode. The dose rates are given normalized to mA-seconds (mA-s) in Tables 2 and 3) to facilitate dose calculations and comparisons to other systems. When expressed in m-As, our measurements are actually total doses, rather than dose rates. However, a dose of 1 mA-s is numerically equal to the dose rate (per second)/mA . A dose of 1 mA-s is just the amount of X-radiation generated when $1 \times 10^{-3}$A/(1 electron charge) = $6.2 \times 10^{15}$ electrons are incident on the X-ray tube anode.

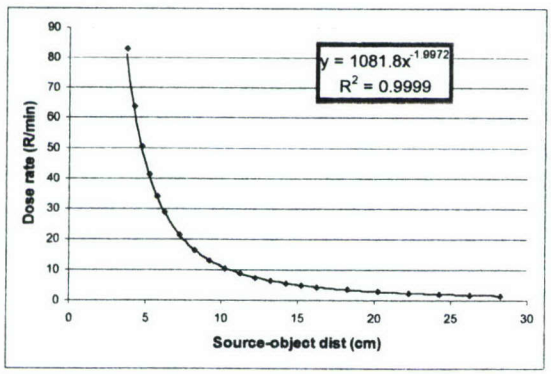


Figure 6. Dose rate vs distance, 100 kV, 80 μA, with 1/16 in. aluminum source filter.

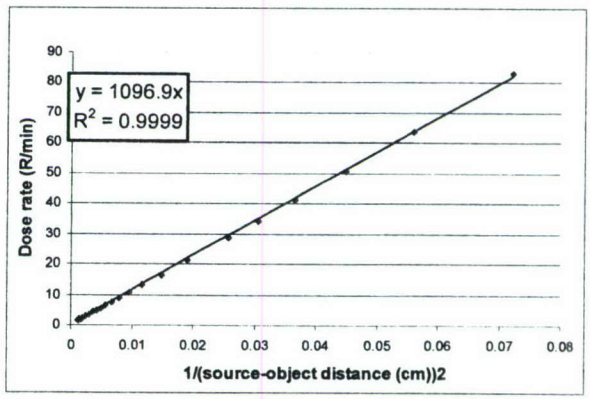


Figure 7. Dose rate vs $1/(\text{source-object distance})^2$, 100 kV, 80 mA with 1/16 in. Al source filter (a replot of the data of Figure 6).

Table 1. Feinfocus System, Dose Rate, No Filter Over Source

| kV | μA | A(R/min) | A(Rad(air)/min) | A(rad(air)/mA-s | N | Fit ($R^2$) |
|---|---|---|---|---|---|---|
| 50 | 160 | 3496.4 | 3062.8 | 319.0 | 2.0326 | 1 |
| 75 | 106 | 3643.6 | 3191.8 | 501.8 | 2.0301 | 1 |
| 100 | 80 | 3455.5 | 3027.0 | 630.6 | 2.024 | 1 |
| 125 | 64 | 3458.7 | 3029.8 | 789.0 | 2.0276 | 1 |
| 150 | 53 | 3174.4 | 2780.8 | 874.5 | 2.0148 | 1 |
| 175 | 45 | 2539.6 | 2224.7 | 824.0 | 2.0054 | 0.9998 |
| 200 | 40 | 1613.2 | 1413.2 | 588.8 | 1.9851 | 0.9993 |

Units of the constant "A" also include a factor of 1 $cm^2$ for source-object distances in cm.

Table 2. Feinfocus System, Dose Rate, 1.6 mm Aluminum Filter Over Source

| kV | μA | A(R/min) | A(Rad(air)/min) | A(Rad(air)/mA-s | N | Fit ($R^2$) |
|---|---|---|---|---|---|---|
| 50 | 160 | 623.7 | 546.4 | 56.9 | 2.0033 | 0.9999 |
| 75 | 107 | 942.77 | 825.9 | 128.6 | 2.0124 | 0.9999 |
| 100 | 80 | 1081.8 | 947.7 | 197.4 | 1.9972 | 0.9999 |
| 125 | 64 | 1338.2 | 1172.3 | 305.3 | 2.0174 | 0.9999 |
| 150 | 53 | 1422.3 | 1245.9 | 391.8 | 2.0118 | 0.9998 |
| 175 | 45 | 1401.1 | 1227.4 | 454.6 | 2.0233 | 0.9998 |
| 200 | 40 | 734.73 | 643.6 | 268.2 | 1.9036 | 0.9994 |

Units of the constant "A" also include a factor of 1 $cm^2$ for source-object distances in cm.

Table 3. Attenuation by 1.6 mm Aluminum Source Filter vs Energy—Feinfocus

| Energy (kV) (8 W power) | Measured dose rate ratio without/with Al source filter |
|---|---|
| 50 | 5.61 |
| 75 | 3.87 |
| 100 | 3.19 |
| 125 | 2.58 |
| 150 | 2.23 |
| 175 | 1.81 |
| 200 | 2.2 |

The measurements in Table 2 were originally made in 1998, and were repeated five years later. Agreement was very good, indicating that the X-ray output is stable with time. The decrease in output at the higher tube voltages was reproduced, and accurately reflects actual tube performance.

Source filtration is common practice in microfocus radiography. We usually use an aluminum filter with our Feinfocus system. The lower energy part of the X-ray spectrum that is removed by the aluminum contributes little to image formation. The photons in the lower energy tail may not even penetrate the sample, and of course must penetrate the sample to form an image. These photons can, however, help saturate the detector.

Tables 1 and 2 show that the $1/r^2$ dependence holds over the range of energies commonly used in our system, with or without source filtering. Table 3 summarizes the differences in dose rates measured with and without the filter.

We should add a minor caveat to the interpretation of Tables 1 and 2. The distance "r" in the $1/r^2$ fits to the measured dose values is the source-to-detector distance. We can easily measure the distance from the face of the X-ray tube to the detector. The actual X-ray source is the elliptical footprint of the tube's electron beam on the cylindrical anode, and is about 6 mm behind the flat face of the tube. The distances measured to the tube face were, therefore, corrected by adding 6 mm to determine the real source-to-detector distances. The ionization chamber is calibrated specifically when oriented with its long axis perpendicular to the X-ray beam, and the detector position was assumed to be at the center of the ionization chamber.

### 3.1.2 Tube Power and Current

Although the Feinfocus tube is generally operated at 8 W to achieve the smallest focal spot, the spot size does not limit image resolution in larger objects. In large samples, features of interest often can not be brought close to the focal spot because of geometric constraints. Image signal-to-noise ratio can then be improved by operating the tube at higher power without, in practice, any penalty in spatial resolution, which is limited by the detector. As expected, the dose rate increases nearly linearly with X-ray tube current (Figure 8). The dose rate also increases with voltage.

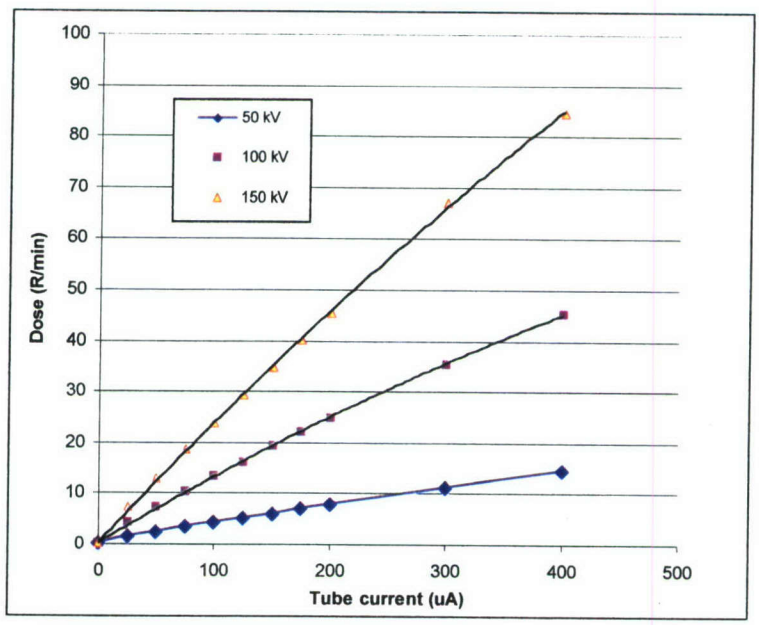


Figure 8. Dose rate vs tube current at constant voltage (with 1.6 mm Al source filter), measurements 10 cm from tube face. Solid lines are 2nd-degree polynomial fits to the data.

### 3.1.3 Angular Distribution

The X-ray radiation pattern is a cone that is ultimately defined by the thick steel head of the Feinfocus X-ray tube. The width of the pattern can be measured by moving the ionization chamber across the beam in the horizontal or vertical direction. The cone angle can be measured even more easily simply by moving the image intensifier closer to the source until the sharp edge of the illuminated cone region can be seen on the video monitor. Both methods lead to a full cone angle of about 30°. The radiation patterns as mapped in Figures 9 and 10 show that the center of our X-ray beam points down and to one side of the center of our detector. Some "shimming" of the tube position was done after installation. As a practical matter, since the image intensifier is normally positioned at just the distance from the source where clipping of the outer edge of the image begins to occur, objects not in the field of view are not being directly irradiated. Within the cone, the radiation intensity does vary. These x-axis and y-axis intensity variations were measured in a plane at 20 cm from the detector. Some of the variation is accounted for by the variation of the source-to-object distance as the detector traverses the measurement plane. For higher magnification imaging of smaller specimens, i.e., at relatively small fields of view, the intensity variation is less noticeable. Variations in source intensity across an image can be removed by post-processing.

## 3.2 Phoenix

### 3.2.1 Dose vs Distance

The X-ray intensities measured as a function of distance from the focal spot, along the center axis of the tube, are summarized in Table 4. The intensity data are again fit to an inverse-square dependence ($A/r^2$). Just as with the Feinfocus system, "r" is the distance from the focal spot to the ionization chamber, and we measure the distance from the face of the tube. Since the focal spot is only about 0.4 mm behind the tube face, the difference is negligible in our fit of the Phoenix data.

The intensity ratios with and without the source filter are shown in Table 5.

### 3.2.2 Dose Versus Tube Current

The radiation intensity in the Phoenix system is a linear function of the tube current, as indicated in Figure 11.

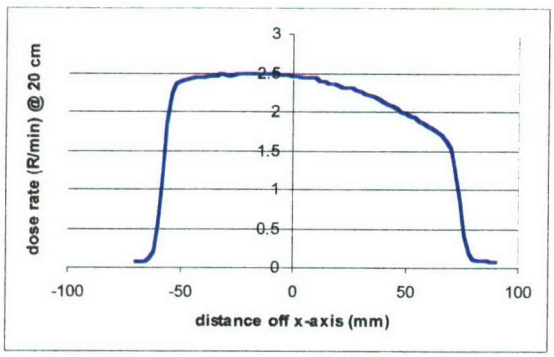


Figure 9. Angular dependence of Feinfocus radiation intensity in a horizontal plane.

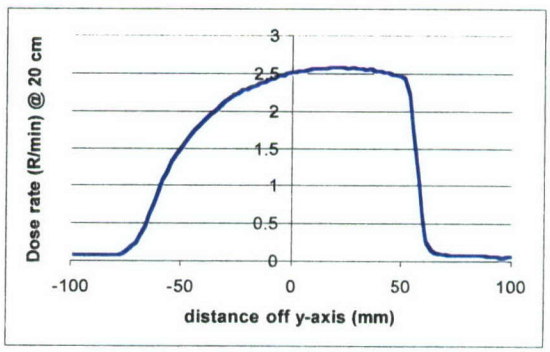


Figure 10. Angular dependence of Feinfocus radiation intensity in a vertical plane.

Table 4. Phoenix System Dose Rates

| kV | μA | A (R/min) | A (Rad(air)/min) | A(Rad(air)/mA-s | n | Fit ($R^2$) |
|---|---|---|---|---|---|---|
| **Without Aluminum Source Filter** | | | | | | |
| 20 | 188 | 151.5 | 132.7 | 11.7 | 1.9922 | 1 |
| 25 | 152 | 295.3 | 258.7 | 28.4 | 1.9956 | 1 |
| 50 | 76 | 1045.6 | 915.9 | 200.9 | 1.9963 | 1 |
| 75 | 51 | 1683.8 | 1475.0 | 482.0 | 2.0198 | 1 |
| 100 | 38 | 1905.3 | 1669.0 | 732.0 | 2.0026 | 1 |
| 125 | 30 | 1925.1 | 1686.4 | 936.9 | 2.0012 | 1 |
| 150 | 24 | 1798.6 | 1575.6 | 1094.1 | 1.9996 | 1 |
| 160 | 24 | 1845.0 | 1616.2 | 1122.4 | 1.9998 | 1 |
| **With 1.6 mm Aluminum source filter** | | | | | | |
| 25* | 152 | 22.7 | 19.9 | 1.76 | 1.9403 | 0.9999 |
| 50 | 75 | 271.1 | 237.5 | 52.8 | 1.9901 | 1 |
| 75 | 50 | 486.5 | 426.2 | 142.1 | 2.0003 | 1 |
| 100 | 38 | 628.2 | 550.3 | 241.4 | 1.9997 | 1 |
| 125 | 30 | 688.5 | 603.1 | 335.07 | 1.9987 | 1 |
| 150 | 25 | 701.5 | 614.5 | 409.7 | 1.9926 | 1 |
| 160 | 24 | 715.2 | 626.5 | 435.1 | 19959 | 1 |

* Source filtering would not normally be used at low voltages
(Units of the constant "A" also include a factor of 1 $cm^2$ for source-object distances in cm)

Table 5. Attenuation by 1.6 mm Aluminum Source Filter vs Energy - Phoenix

| Energy (kV) (3.8 W power) | Measured dose rate ratio without/with Al source filter |
|---|---|
| 25 | 13.0 |
| 50 | 3.85 |
| 75 | 3.46 |
| 100 | 3.03 |
| 125 | 2.80 |
| 150 | 2.56 |
| 160 | 2.58 |

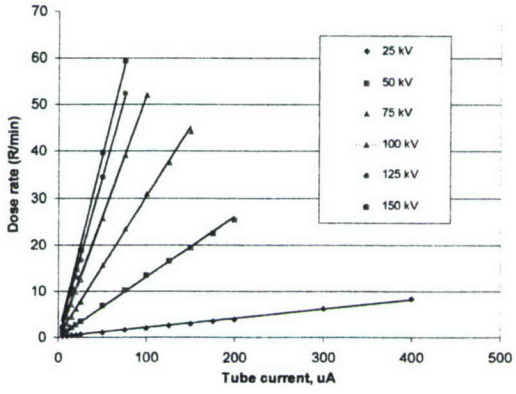


Figure 11. Dose rate vs tube current for a transmission X-ray tube.

### 3.2.3 Angular Distribution

The radiation intensity was measured along a line perpendicular to the tube axis in a plane (i.e., on the specimen table) by translating the table (Figure 12). The sample table was 5 cm from the X-ray source.

### 3.2.4 Nanofocus Mode

Maximum accelerating potential is limited to 100 kV in the nanofocus mode. The focal spot size is stated in the manufacturer's specifications to be about 0.6 μm. The dose rates measured in nanofocus mode are given in Table 6.

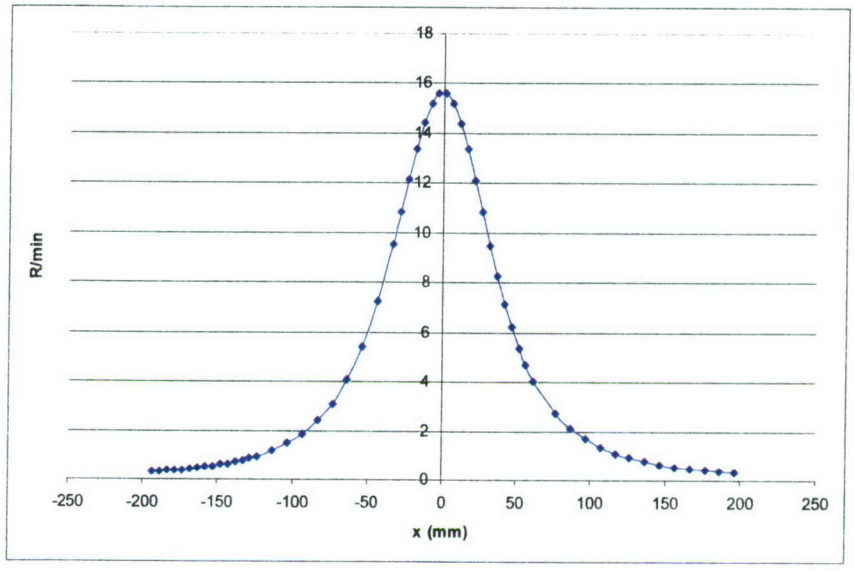


Figure 12. Phoenix angular distribution (dose rate vs distance from tube axis).

Table 6. Phoenix Nanofocus Mode

| kV | μA | A(R/min) | A(Rad(air)/min | A(Rad(air)/mA-s | n | Fit ($R^2$) |
|---|---|---|---|---|---|---|
| **Without Aluminum Source Filter** | | | | | | |
| 25* | 140 | 14.0 | 12.3 | 1.46 | 1.9535 | .9994 |
| 50 | 70 | 44.3 | 38.8 | 9.24 | 1.9808 | .9999 |
| 75 | 46 | 88.0 | 77.1 | 27.9 | 2.0079 | .9999 |
| 100 | 35 | 109.0 | 95.5 | 45.5 | 2.002 | 1 |
| **With 1.6 mm Al source filter** | | | | | | |
| 25* | 140 | 0.72 | 0.63 | .08 | 1.9535 | .9989 |
| 50 | 70 | 6.92 | 6.6 | 1.4 | 1.9808 | .9998 |
| 75 | 46 | 16.09 | 14.1 | 6.7 | 2.0079 | .9999 |
| 100 | 35 | 23.79 | 20.8 | 9.9 | 2.002 | .9998 |

*Source filtering would not normally be used at low voltages.

Units of the constant "A" also include a factor of 1 $cm^2$ for source-object distances in cm)

# 4. Discussion

The measurements presented characterize both an X-ray system based on a directional tube (Feinfocus) and a system (Phoenix) that incorporates a transmission-type tube. The first question that one might ask is whether the measured numbers for dose rates are reasonable; i.e., can we do a sanity check? We would like then to go further and understand the interpretation of the experimental measurements in more detail. In particular, we would like to be able to estimate doses in silicon and other materials of particular interest in microelectronics.

We have been talking in terms of the energy used in X-ray analysis. Tube voltage (energy) and tube current are knobs on the control panels of most X-ray systems. However, the spectrum generated by an X-ray tube is not monochromatic, and the interaction of X-ray photons with matter is strongly dependent on their energy. The physics underlying the generation, transmission, and absorption of X-rays is completely understood. In principle, our measurements can be checked, and all of our questions answered, through computation. This approach, as we shall see, works in practice as well. This is not to say that the physics is necessarily simple, but it is well known. There are a number of computer programs available to carry out these calculations, and some of these programs are available at no cost. Tucker, Barnes, and Chakraborty (TB&C) have published simulation routines for X-ray tubes with tungsten[2] and molybdenum[3] anodes. The computed spectra closely emulate experimental results obtained from a number of medical tubes. TB&C incorporate both the Bremsstrahlung radiation that is produced when charged particles are accelerated in the field of nuclei and the characteristic emission lines associated with the excitation of discrete atomic energy levels in tungsten targets. A computer program that implements the TB&C algorithms can be downloaded from the University of Toronto.[4] These papers, and the U. of Toronto's implementation of (and improvements to) the code, provide a good starting point for the exploration of X-ray tube spectra. Other semi-empirical models give comparable results.[5] Semi-empirical models are necessarily limited in scope. Essential features are hard-wired into the programs and can't easily be changed. Electron-photon transport codes, on the other hand, are more general, but are harder to use. Codes based on the solution of the differential Boltzmann transport equation and on Monte Carlo methods are available. Popular Monte Carlo codes include PENELOPE,[6] GEANT4,[7] MCNP,[8] and EGSnrc/BEAMnrc[9,10] (BEAMnrc is intended for the modeling of sources, while EGSnrc is directed toward dose calculations). Monte Carlo methods have been used by a number of researchers to model both diagnostic and industrial microfocus X-ray systems operating around 100 kV.[11,12,13,14] We will use both the TB&C model and BEAMnrc in the discussion of our measurements.

## 4.1 X-ray Tube Model

Simplified models of the X-ray tubes were used in our calculations. The X-ray tubes were modeled in BEAMnrc, as indicated in Figure 13. The anode is a cylinder not a flat surface, but, in practice, for a small beam spot, this detail is not an issue. The transmission tube geometry has also been simplified, but again these simplifications don't seem to matter. TB&C also model the directional tube anode as flat, with some different definitions of the angles. The TB&C model is not set up to handle

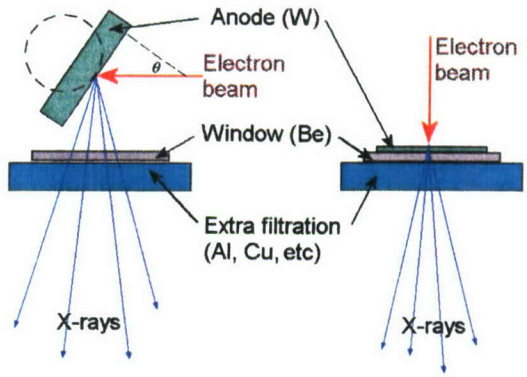


Figure 13. Our directional tube model is shown at the left, and our transmission tube model at the right.

transmission tubes. Monte Carlo codes could be extended to take most details of tube structure into account if desired, but the simplified models seem adequate for our purposes.

Typical X-ray spectra calculated using both TB&C and BEAMnrc are shown in Figure 14. The tube potential is 100 kV, and the exposure is 1 mA-s. A 1.6-mm Al filter is in place. The spectra are in good agreement. These calculations yield not only the spectral shapes but the amplitudes (in photons/ $mm^2$/MeV) as well. Spectra are very similar for transmission tubes. The characteristic $K_\alpha$ and $K_\beta$ peaks around 59 and 67 keV are the most noticeable features of these tungsten-target spectra. The applied voltage is usually abbreviated "$kV_p$" (kilovolts, peak). No X-rays can be produced with energy greater than the applied potential ($kV_p$), as Figures 14 and 15 indicate. Contemporary microfocus systems have well-regulated and filtered power supplies, and $kV_p$ is a well-defined quantity.

We can now inquire more closely about the effects of source filtration. Spectra of a directional tube computed using BEAMnrc with and without a 1.6 mm (1/16 in.) aluminum source filter are shown in

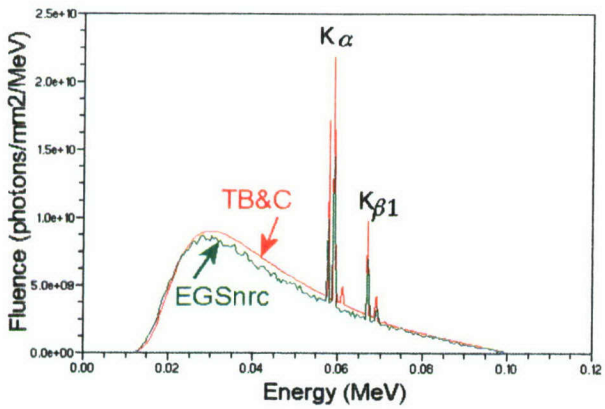


Figure 14. X-ray spectra calculated for a directional tube operated at 100 kV. The exposure was taken to be 1 mA-s, and the source-detector distance is set to 1 m.

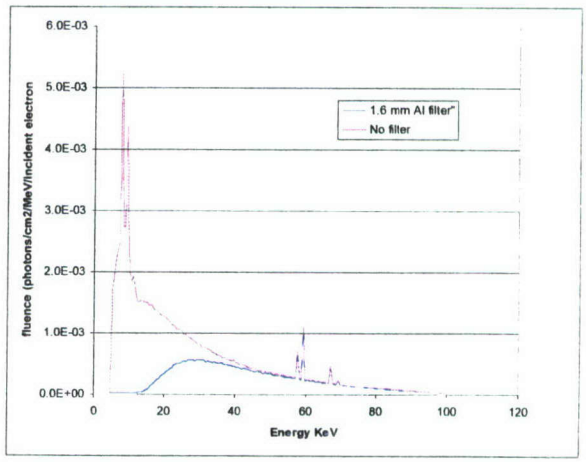


Figure 15. Directional tube spectra calculated using BEAMnrc.

Figure 15. In addition to the characteristic K lines, characteristic L lines appear around 8–10 keV. These peaks are simply not included in the TB&C model. They are very effectively removed by the aluminum filter. Agreement with our dosimetric measurements is improved by source filtration. Neither the TB&C model nor BEAMnrc do a great job for simulations at low (<10 kV) photon energies. BEAMnrc is, however, steadily being extended to lower energies. The essential effects of source filtering can still be seen with either computational method. Other materials can, of course, be used as filters. We often place a piece of copper tape over the exit aperture of the Phoenix system. The 35-μm (0.0014-in.) copper layer gives a spectrum very similar to that obtained with 1.6-mm aluminum. Filtering can be tailored to optimize image quality in particular situations. Source filtering is useful to reduce the total dose to a sample since the lower energy part of the spectrum may not get through the sample and thus may not contribute to image quality. The attenuation of lower energy components of a spectrum is termed "beam hardening." The beam hardening effect is particularly important in computed tomography (CT) and results in well-known artifacts in reconstructed images. Appropriate source filtration can reduce these artifacts. CT is not discussed in this report.

X-ray spectra can be measured directly with energy-selective detectors. What we measure with the ionization chamber is a weighted integral of the energy distribution curve.

## 4.2 Interaction of X-rays With Matter

The intensity of X-radiation decreases exponentially with distance (s) when passing through matter, i.e.,

$$I = I_0 \exp\left(-\left(\frac{\mu}{\rho}\right)\rho s\right), \tag{2}$$

where the linear attenuation coefficient, μ, has been normalized by dividing by the material density. The quantity $(\mu/\rho)$ has the dimensions of $cm^2/g$, while $x = \rho s$ (with dimensions of $gm/cm^2$) is termed the mass thickness. X-ray imaging requires that photons neither be absorbed completely (the image would be totally dark) or transmitted without loss (the sample would not show up at all against a completely bright field). X-ray energy must be adjusted to meet these conditions. Tables of attenuation coefficients are available from the National Institute of Standards and Technology(NIST).[15] The NIST tables and accompanying graphs present two quantities, the mass attenuation coefficient $(\mu/\rho)$ and the mass absorption coefficient $(\mu_{en}/\rho)$. It is indeed true that the density terms cancel in Eq. (2), but, expressed in this way, the tabulated data are normalized in a numerically convenient manner. X-ray photons interact with matter in the range of our available X-ray energies through photoelectric interactions and through coherent and incoherent scattering. In each of these processes, only a fraction of the energy is transformed into the kinetic energy of charged particles. The mass energy absorption coefficient further takes into account any additional energy that is removed from the specimen through the generation of additional photons. The fraction of incident energy deposited in a thin slice of material of thickness Δs normal to an incident X-ray beam is given by

$$\frac{\Delta I}{I} = -\left(\frac{\mu_{en}}{\rho}\right)\rho\Delta s\,. \tag{3}$$

The attenuation of an X-ray beam may result either from processes that deposit energy in the sample or from processes in which energy (in the form of photons) is reemitted and lost by scattering. For calculations of attenuation, the mass attenuation ($\mu/\rho$) is the relevant quantity. For energy deposition, ($\mu_{en}/\rho$) is the relevant quantity.

The air dose in Roentgens is calculated from the photon flux by summing the product of the fluence (photons/area) and the mass absorption coefficient over all spectral energies, i.e.,

$$R = \frac{e(1.0\text{x}10^{-8})}{I_p(2.58\text{x}10^{-4})} \sum_{\text{bins}} \left( \frac{\mu_{en}}{\rho} \right)_{\text{air}} E(\text{keV}) \Phi(\text{photons}/\text{mm}^2/\text{bin}), \qquad (4)$$

where $\Phi$ is the number of photons of energy E per energy bin, and $(\mu_{en}/\rho)_{air}$ is again the mass absorption coefficient for air. A photon of energy, E, is assumed to generate $E/I_p$ ions. $I_p$ = 33.97 eV is the average ionization energy of air. "e" is the electronic charge, and 1 R = 2.58 x $10^{-4}$ coulombs/kg of air. The factor 1 x $10^{-8}$ takes care of some necessary unit conversions. This is essentially the notation used by the TB&C code, which incorporates this algorithm and delivers dose in R along with the calculation of the spectrum. The summation is over the energy bins into which the spectrum is divided in the calculation. For the dose in Rad(air), the numerical constant in front of the summation symbol becomes $10^{10}$*1.602 x $10^{-19}$. Although EGSnrc will calculate energy depositions directly, photon by photon, Eq. (4) has also been used in the present work to derive doses from EGSnrc spectra in order to save computing time.

### 4.3 Comparisons With Experiment

Do the measured doses agree with experiment? Microfocus tubes are effectively point X-ray sources. Measuring dose as a function of distance is a convenient way to fit a tube's dose parameter. However, the $1/r^2$ dependence that is observed is dictated by Gauss's law. It's required by physics, *unless* the air along the source-to-sample path scatters or absorbs a significant fraction of the X-rays. The effect of ambient air is certainly negligible over the 10's-of-centimeter dimensions typical of our Feinfocus and Phoenix "cabinet" X-ray systems, especially for beams hardened by typical source filters such as 1.6 mm of aluminum. At very low energies (≤50 kV), where source filtering might not be used, some departure from $1/r^2$ behavior could be expected for large (10's of cm to meters) distances (Figure 16). Such deviations were not observed in the present work (the X-ray cabinet enclosures aren't large enough).

Figure 17 shows the dose rate vs. tube current data presented earlier in Figure 8 for the Feinfocus instrument. The added dashed straight lines are calculated using TB&C. The agreement with experiment is quite good at low currents although the measured doses "droop" a bit at high current. Both TB&C and BEAMnrc scale their results linearly with the number of electrons incident on the anode; straight lines as a function of tube current are guaranteed. A possible explanation of is that the electron beam may shift about on the cylindrical anode as beam current increases and cause the observed sag in the Feinfocus tube output. The X-ray output of the Phoenix system (Figure 11) is quite linear with tube current. The electron beam in a transmission tube is perpendicular to the anode, and this simpler geometry could account for the more linear behavior compared to a directional tube.

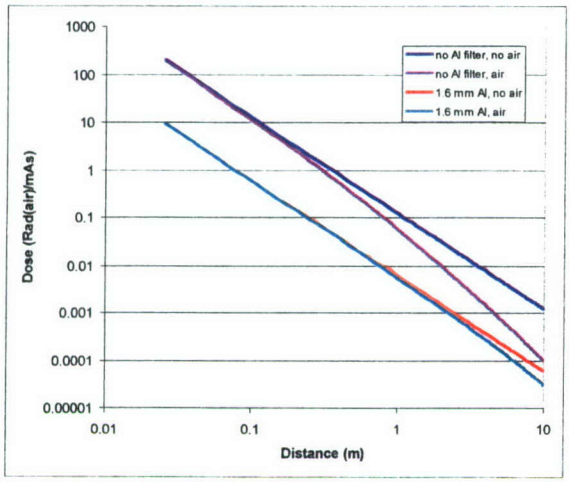


Figure 16. Dose vs source-detector distance for 50-kV X-rays, calculated using TB&C for a vacuum or an air path, and with and without a 1.6 mm Al filter.

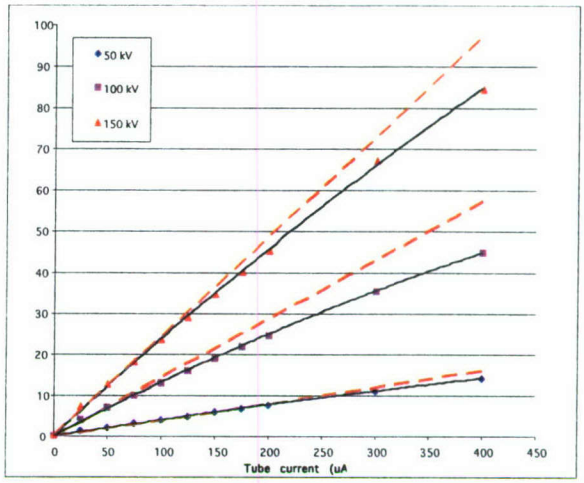


Figure 17. The dose vs tube current data for tube potentials of 50, 100, and 150 kV (presented earlier). The straight lines are calculated from TB&C.

As mentioned earlier, the TB&C model applies to directional tubes rather than transmission tubes. For the Phoenix system, we obtained very reasonable results for doses using BEAMnrc, as shown in Table 7 for 10 cm source-object distance. The "measured" values are taken from Table 4 with r = 10 cm. A 1.6-mm aluminum source filter is assumed. Although the measured Feinfocus doses have been quite stable over the years, the Phoenix doses do seem to have drifted a bit lower. In general, however, agreement between experiment and theory is good.

The spatial distribution of the radiation from our X-ray tubes can also be calculated using Monte Carlo methods. In Figure 18, we again show the experimental data for the Phoenix system. We have superimposed the angular distribution at 100 kV as calculated by BEAMnrc. The result most readily accessible from BEAMnrc gives an energy fluence (MeV/incident particle/cm$^2$) as a function of radial distance rather than a dose in R or Rad(air). These data were simply scaled to fit the experimental curve. The calculated distribution does fall off a bit more rapidly with distance from the tube centerline, but is a reasonable match to the shape of the experimental curve. Note, however, that much of this observed variation in intensity is simply a consequence of the $1/r^2$ dependence of the source-to-sample distance as the detector is translated, on the sample stage, away from the tube centerline. The tube-to-table distance remained fixed at 50 mm. Non-relativistic electrons radiate preferentially

Table 7. Comparison of Measured vs Computed Doses for Phoenix System

| kV | Rad(air)/mA-s (measured) | Rad(air)/mA-s (BEAMnrc) |
|---|---|---|
| 25 | 0.02 | 0.04 |
| 50 | 0.53 | 0.49 |
| 75 | 1.42 | 1.27 |
| 100 | 2.41 | 2.26 |
| 125 | 3.35 | 3.26 |
| 150 | 4.10 | 4.06 |

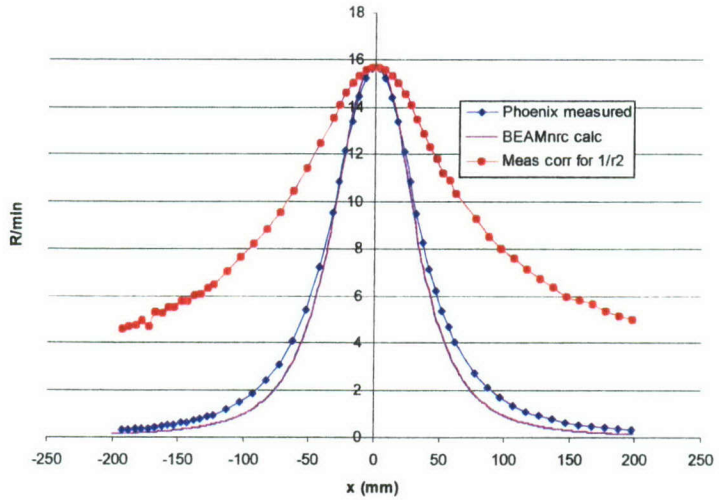


Figure 18. Measured spatial distribution of radiation from Phoenix system 5 cm from source at 100 kV, with scaled BEAMnrc calculation (red) superimposed. Broader distribution is for measured distribution corrected for $1/r^2$ dependence.

perpendicular to their direction of motion as they decelerate. One would expect the radiation from a transmission tube to have a broad angular distribution. When corrected for distance, the measured distribution indeed looks rather broad. The radiation intensity was measured as a function of angle at fixed source-to-detector distance by affixing the ion chamber probe to a spacer attached to the center of the Phoenix system's solid-state detector (see Figure 19). A Gaussian fit indicates a full pattern width at half maximum of about 100°. The Phoenix instrument manual states that the full cone angle is 170°, although the manner in which this quantity is defined is unclear. Again, measurements are in satisfactory agreement with theory.

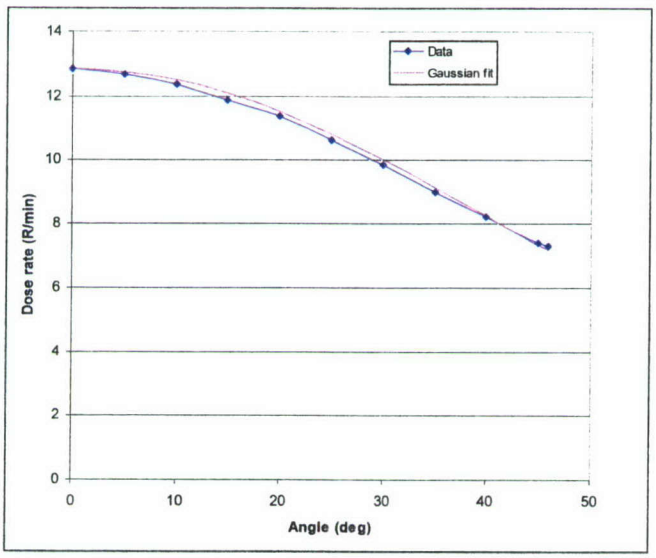


Figure 19. Dose rate as a function of angle at fixed (53.6 mm) source to ionization chamber distance. A Gaussian with a full width at half maximum of 100° yields a reasonable fit.

Other features of our X-ray tubes can also be understood based on our models. For example, the anode in the Phoenix transmission tube is a layer of tungsten 6 μm thick on a beryllium support. It is clear that few X-rays would be produced in the limit as the tungsten layer goes to zero thickness. It is also evident that if the anode layer were sufficiently thick, any X-rays generated would be reabsorbed before exiting. There is, therefore, an optimum anode thickness. For a tube operating at 100 kV, Monte Carlo calculations indeed show that X-ray output is maximum for a 6-μm-thick tungsten anode. X-ray generation is less efficient at lower and higher voltages, but 6 μm is a good compromise. More subtle details, such as the "heel effect," can also be investigated and explained by CB&T or Monte Carlo methods.[16] The heel effect is an intrinsic asymmetry associated with a directional tube geometry that results from the relatively shorter path that X-rays must travel to exit the anode on the cathode side.

The details of nanofocus tube design are not well documented. Table 6 shows that the X-ray output is significantly lower at comparable power levels. The anode is presumably thinner by design in the nanofocus anode of the Phoenix system for which the tube potential is limited to a maximum of 100 kV.

### 4.4 Doses in Materials Other Than Air

The absorbed dose in materials other than air can be readily calculated. For silicon, one finds:

$$\mathrm{Rad(Si)} = (10^{10} \cdot 1.602 \cdot 10^{-19}) \sum_{\mathrm{bins}} \left( \frac{\mu_{en}}{\rho} \right)_{\mathrm{Si}} \mathrm{E(keV)} \Phi(\mathrm{photons/mm^2/bin}). \qquad (5)$$

This expression assumes a thin absorber.

For a 10-μm-thick silicon absorber, the thin-sample approximation is valid; i.e., the attenuation length attenuation $1/\mu_{en}$ is large compared to the sample dimensions At 4.7 cm from the source, we find the doses given in Table 8 for a thin absorber in the Feinfocus system (with a 1.6 mm Al source filter in place). Table 8 serves as a guide to the absorbed dose in Rad(Si) that will be received by a thin silicon sample. The short answer is that the dose in Rad(Si) is about 6 to 8 times the dose expressed in Rad(air).

Table 8. Dose in Air vs. Dose in Silicon

| kV | Rad(Si)/Rad(air) |
|---|---|
| 50 | 8.23 |
| 75 | 7.94 |
| 100 | 7.52 |
| 125 | 7.11 |
| 150 | 6.70 |
| 175 | 6.31 |
| 200 | 5.94 |

The dose rate near boundaries in multiplayer materials can be increased significantly above the equilibrium dose. Dose "leakage," i.e., a decrease in local dose attributable to secondary-electron generation, can also occur. Figure 20 shows the calculated dose in a 25-mm-thick slice of silicon compared to the dose in the silicon with a 0.5-μm-thick gold layer on top. A spectrum calculated using BEAMnrc was used as input to the dosxyznrc program that computes doses for rectangular geometries. The dosxyznrc program is part of the EGSnrc/ BEAMnrc suite.[9] The incident X-rays here are assumed to be in a parallel X-ray beam with the spectrum calculated for a tungsten target with a peak energy of 100 keV. Such a sample geometry is typical of what might be encountered in an integrated circuit. The dose is higher in the silicon just below the gold by a factor of about 17 than it would be in the uncoated silicon. As an additional check, results from a commercial dose calculation program, PHOTCOEFF, were found to be in agreement with the Monte Carlo calculations of Figure 20.[17] PHOTCOEFF is relatively easy to use, but it is a "black box" package that uses proprietary algorithms.

## 4.5 Computational Considerations

The TB&C calculations run very quickly on modern personal computers The University of Toronto implementation was written for Matlab. We adapted the code to run under Scilab, a similar but freely downloadable programming environment.[18] We also changed the code to incorporate construction materials more typical of industrial microfocus tubes (e.g., copper and beryllium) rather than materials more commonly used in medical X-ray systems (e.g., lexan and mineral oil).

Monte Carlo calculations are much more computer intensive. We run EGSnrc/BEAMnrc on a Linux cluster with 22 Pentium IV processors operating at 3.6 GHz. Computation times are typically minutes to tens of minutes.

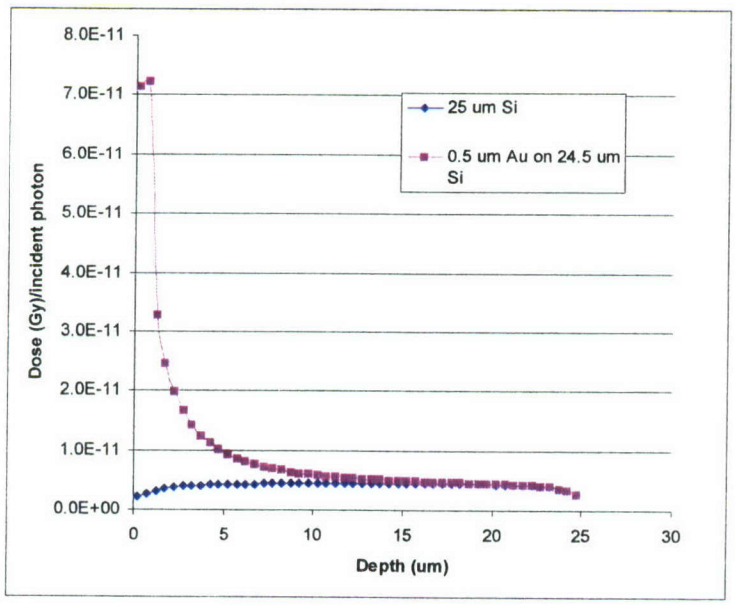


Figure 20. EGSnrc calculation of dose relative dose in silicon with (blue triangles) and without (purple circles) an overlying 0.5-μm-thick gold layer.

## 4.6 Thermoluminescent Dosimetry and Other Measurement Methods

Several other methods of radiation measurement were explored. Thermoluminescent dosimeters (TLDs) are based on the fact that ionizing radiation creates defects in crystal lattices. Some materials, such as lithium fluoride, emit part of the energy stored in these defects as light when they are heated after irradiation. The amount of light emitted is proportional to the X- or gamma radiation dose received by the crystal. TLDs are commercially available as encapsulated powders and as small (e.g., 0.125 in. square by 0.035 in. thick) crystals. The small crystals are convenient because they can be placed inside electronic assemblies. The TLDs must be returned to the vendor for readout. Commercial providers of dosimetric services offer to report results in any unit requested by the customer, including rad(Si). We probed a bit further with one supplier. Most of their samples were personal dosimeters used for personnel safety monitoring. Their dosimeter readouts were said to be traceable to the National Institute of Standards and Technology for personnel monitoring (i.e., for radiation doses deposited in flesh or water). As best as could be determined in a telephone conversation, our vendor's correction to get to rad(Si) was made with a "plug-in" spreadsheet. The correction factor being employed was appropriate for 1.25-MeV monochromatic gamma rays but not for radiographic X-rays. Another complication is that the total dose needs to be known approximately in order to preset the gain of the readout device (at least in this vendor's instrument), otherwise accuracy is compromised. This episode is recounted as a cautionary tale.

A direct approach to measuring doses in silicon is to use silicon as a detector. Silicon p-type/insulator/n-type (PIN) diodes have been used for dose measurements, as have bipolar transistors and metal-oxide semiconductor field effect transistors.[19]

## 4.7 Minimization of Total Dose

We have seen that the dose received by a specimen depends on the X-ray tube voltage and current, the source-specimen distance, the filtration of the X-radiation, and the exposure time. These parameters can be manipulated to reduce total dose. Increasing the source-specimen distance reduces the dose, but also decreases the magnification. One must make trade-offs. Image contrast resolution depends on tube current and voltage, as well as the source filtration. Here again, tradeoffs are involved if dose is to be reduced. The most efficacious strategy is often simply to minimize the time spent looking at a sample. Start with a practice part (perhaps an extra part from stores or a non-flight component). Set up the imaging parameters and define the areas of interest. The work on the "real" samples is then done as quickly as possible to ensure that total dose limits are not exceeded. This tactic may not work well if a complex component or an assembly representing a one-of-a-kind failure has to be inspected. Finally, if only certain areas of a sample need to be examined, other regions might be shielded with lead foil.

## 5. Summary

The output of microfocus X-ray tubes is basically determined by the applied voltage and the electron beam current. The construction details of particular tubes are not all that important, although somewhat different dose numbers are obtained for directional and for transmission-type tubes. This assertion depends on the fact that the same laws of physics apply equally to all manufacturers. For any given X-ray system, experimental measurements are always desirable, but the available tube models should adequately describe tube output.

Tables 1 and 2, for a directional tube (Feinfocus), and Tables 4 and 5, for a transmission tube (Phoenix), respectively, summarize much of the essential information in this report, viz., the dose as a function of voltage, tube current, and source-detector distance. These tables provide a starting point for determining the dose in directional or transmission tubes. A calibrated ionization chamber meter should provide a "sanity check" and verify that a system is operating properly. It would be prudent to characterize the output of a new X-ray system and make periodic measurements thereafter. A significant drop in output would likely first be evident as a loss in image quality.

Available semi-empirical tube models and Monte Carlo electron-photon transport codes are consistent with measured values. Doses in materials other than air can be calculated if values in air are known. Thermoluminescent dosimeters (TLDs) can be used if direct dose measurements in small spaces are needed. The dose values reported by vendors for TLDs, in our experience, may sometimes be open to question. At the risk of stating the obvious, TLDs should always be submitted for readout with calibration standards that have been exposed to the direct X-ray beam and validated with a calibrated meter. *Remember to ask the vendor to report the results in units of both rad(air) and rad(semiconductor)!*

The actual dose in localized regions of a semiconductor may be enhanced by the presence of layers of materials of high density. Customers with concerns about radiation damage in an X-ray inspection will usually quote some number, in kRad(Si), that should not be exceeded. If their parts have been tested by exposure to X-rays of the same general energy (~100 $kV_p$ ) as analytic X-rays, then the various dose enhancement effects will hopefully have already been factored in.

This report has discussed doses that can be expected in microfocus X-ray examinations using the "conventional" commercial systems available in 2007. These systems employ focused electron beams that impinge on tungsten anodes to generate small-spot sources of X-rays. X-ray tubes have been improved incrementally over the past decade. New technology for 2-dimensional and 3-dimensional (CT) imaging based on Fresnel zone plate X-ray optics is now on the market. The future applications of radiographic imaging in the aerospace and allied industries promise to be very interesting.

## References


1. Radcal Corporation, 426 W. Duarte Road, Monrovia, CA 91016 (www.radcal.com)
2. Tucker, D. M, G. T. Barnes and D. P. Chakraborty, *Med. Phys.* **18**, 211–218 (19911).
3. Tucker, D. M., G. T. Barnes and X. Wu, *Med. Phys.* **18**, 402–407 (1991).
4. http://www.ecf.utoronto.ca/apsc/courses/bme595f/index.html
5. J. M. Boone and J. A. Seibert, *Med. Phys.* **24**, 1661–1670 (1997).
6. http://www.nea.fr/abs/html/nea-1525.html
7. http://geant4.web.cern.ch/geant4/
8. http://mcnp-green.lanl.gov/index.html
9. http://www.irs.inms.nrc.ca/EGSnrc/EGSnrc.html
10. http://www.irs.inms.nrc.ca/BEAM/beamhome.html
11. L. M. N. Tavora and E. J. Morton, Nucl. Sci. Symp. 1996, *IEEE*, **2**, 783–787 (1996).
12. F. Verhaegen, A. E. Nahum, S. Van de Putte and Y. Namito, *Phys. Med. Biol.* **44**, 1767–1789 (1999).
13. L. M. N. Tavora, E. J. Morton, F. P. Santos and T. H. V. T. Dias, *IEEE Trans. Nucl. Sci.* **27**, 1493–1498 (2000)
14. D. W. O. Rogers, *Phys. Med. Biol.* **51**, R287–R301 (2006).
15. http://physics.nist.gov/PhysicsRefData/XrayMassCoef/cover.html
16. M. Bhat, J. Pattison, G. Bibbo and M. Caon, *Med. Phys.* **26**, 303–309 (1999).
17. AIC Software, Inc., P.O. Box 544, Grafton, MA 01519
18. www.scilab.org
19. R. D. Bellem, K. L. Critchfield, R. M. Pelzl, R. D. Pugh and R. W. Tallon, *IEEE Trans. Nucl. Sci.* **41**, 2139–2146 (1994).

## LABORATORY OPERATIONS

The Aerospace Corporation functions as an "architect-engineer" for national security programs, specializing in advanced military space systems. The Corporation's Laboratory Operations supports the effective and timely development and operation of national security systems through scientific research and the application of advanced technology. Vital to the success of the Corporation is the technical staff's wide-ranging expertise and its ability to stay abreast of new technological developments and program support issues associated with rapidly evolving space systems. Contributing capabilities are provided by these individual organizations:

**Electronics and Photonics Laboratory:** Microelectronics, VLSI reliability, failure analysis, solid-state device physics, compound semiconductors, radiation effects, infrared and CCD detector devices, data storage and display technologies; lasers and electro-optics, solid-state laser design, micro-optics, optical communications, and fiber-optic sensors; atomic frequency standards, applied laser spectroscopy, laser chemistry, atmospheric propagation and beam control, LIDAR/LADAR remote sensing; solar cell and array testing and evaluation, battery electrochemistry, battery testing and evaluation.

**Space Materials Laboratory:** Evaluation and characterizations of new materials and processing techniques: metals, alloys, ceramics, polymers, thin films, and composites; development of advanced deposition processes; nondestructive evaluation, component failure analysis and reliability; structural mechanics, fracture mechanics, and stress corrosion; analysis and evaluation of materials at cryogenic and elevated temperatures; launch vehicle fluid mechanics, heat transfer and flight dynamics; aerothermodynamics; chemical and electric propulsion; environmental chemistry; combustion processes; space environment effects on materials, hardening and vulnerability assessment; contamination, thermal and structural control; lubrication and surface phenomena. Microelectromechanical systems (MEMS) for space applications; laser micromachining; laser-surface physical and chemical interactions; micropropulsion; micro- and nanosatellite mission analysis; intelligent microinstruments for monitoring space and launch system environments.

**Space Science Applications Laboratory:** Magnetospheric, auroral and cosmic-ray physics, wave-particle interactions, magnetospheric plasma waves; atmospheric and ionospheric physics, density and composition of the upper atmosphere, remote sensing using atmospheric radiation; solar physics, infrared astronomy, infrared signature analysis; infrared surveillance, imaging and remote sensing; multispectral and hyperspectral sensor development; data analysis and algorithm development; applications of multispectral and hyperspectral imagery to defense, civil space, commercial, and environmental missions; effects of solar activity, magnetic storms and nuclear explosions on the Earth's atmosphere, ionosphere and magnetosphere; effects of electromagnetic and particulate radiations on space systems; space instrumentation, design, fabrication and test; environmental chemistry, trace detection; atmospheric chemical reactions, atmospheric optics, light scattering, state-specific chemical reactions, and radiative signatures of missile plumes.

THE AEROSPACE CORPORATION
2350 E. El Segundo Boulevard
El Segundo, California 90245-4691
U.S.A.